

Gravitational measurements in Non-commutative spaces

Majid Karimabadi, S. Aliasghar Alavi ¹, Davood Mahdavian Yekta

Department of Physics, Hakim Sabzevari University, P.O. Box 397, Sabzevar, Iran

Abstract

The general theory of relativity is the currently accepted theory of gravity and as such, a large repository of test results has been carried out since its inception in 1915. However, in this paper we will only focus on what are considered as the main tests but in non-commutative geometries. Using the coordinate coherent state formalism, we consider gravitational red-shift, deflection, and time delay of light, separately, for *Schwarzschild* and *Riessner-Nordström* metrics in their non-commutative form. We will schematically show that these non-commutative calculations have different behavior with respect to the predictions of general relativity. We also specify an upper bound on the non-commutative parameter by comparing the results with accuracies of gravitational measurements for typical micro black holes which can be produced in the early universe.

¹s.alavi@hsu.ac.ir

1 Introduction

After Einstein published his special theory of relativity in 1905, the next step was to generalize his theory to include non-inertial reference frames; that is, to include acceleration and gravity. Later in 1915, Einstein published a paper in which he was in the first stages of generalizing his theory of relativity to gravity. His theory changed fundamentally our understanding of space-time, mass, energy, and gravity. This theory can be used to predict many new features from the existence of black holes, one of the most interesting and mysterious objects in the universe to the gravitational lensing, red-shift and gravitational time dilation, i.e., the three profound implications of Einsteins general relativity. For further study one can see the textbooks in Refs. [1] - [6].

Gravitational red-shift is a very useful tool in astrophysics. It helps us to test our knowledge of the structure of those stars whose internal structures are different from the sun and other normal stars. Gravitational red-shift gives us the ratio of the stars mass to its radius. Another important prediction of Einsteins general theory of relativity is the deflection of light rays passing close to a massive body. This phenomenon is called gravitational lensing and for the first time, confirmed by Eddington [7]. About one century after the first measurement of the bending of light by the sun, gravitational lensing is still one of the major tools of cosmology [8], astrophysics [9,10] and astronomy [11]. It offers one of the useful tools for probing extra solar planets and to detect the presence and distribution of dark matter which act as sources of the gravitational field [12]. It can also be considered a natural telescope for observing distant galaxies, and to obtain an estimation of the Hubble constant. Statistical study of lensing data provides very useful insight into the structural evolution of galaxies [13,14].

So far General Relativity (GR) has been tatsted on scales smaller than an individual galaxy, e.g., orbits of planets in our solar system and the motion of stars around the center of the Milky way, but recently, it is shown in Ref. [15] that GR also works well on galactic scale. Using data from the Hubble space telescope they found that a nearby galaxy dubbed ESO 325-G 004, is surrounded by a ring like structure known as Einstein ring, which is an evident for gravitational lensing. This precise test of GR on a galactic scale excludes some of the alternative theories of gravitation.

Moreover, gravitational time dilation measures the amount of time that has elapsed between two events by observers at different distances from a gravitational mass. To sum up, the clock placed in a higher gravitational potential region will run slower because the effect of gravity on light will be minimal and the light will take lesser time to reach the reflecting surface. This will in turn make the clock tick slower. Gravitational time dilation has been confirmed by the PoundRebka experiment [16], observations of the spectra of the white dwarf Sirius B, and experiments with time signals sent to and from Viking 1 Mars lander. Time dilation corrections are also very important in Global Positioning System (GPS) [17]. The clocks on GPS satellites tick faster than the clocks on Earths surface, so we have to put a correction into the satellite measurements.

On the other hand, motivated by the string theory [18–21], generalized uncertainty principle [22], quantum gravity [23], Lorentz violation [24, 25], and etc., the idea of non-commutativity of space has drawn quite a lot of interest in a wide range of areas from condensed matter physics to cosmology, high energy physics, and astrophysics. In a number of scenarios in string theory based on the large extra-dimensions there is a bound on the unification scale, thus, if non-commutative (NC) geometry as a promising alternative is induced by string theory, the corresponding length scale should be satisfied in this bound [26, 27]. These ideas offer exciting, near future, possibility of experimentally probing both non-commutativity and quantum gravity effects.

The NC space is realized by the coordinate operators satisfying:

$$[x_i, x_j] = i\theta_{ij}, \quad (1.1)$$

where θ_{ij} is an anti-symmetric tensor which for later convenience we name it NC parameter. The main mathematically correct, but physically hard to implement, formalism for study the non-commutativity is the star-product or Moyal product approach [19]. But there is an alternative approach based on the coordinate coherent states [28, 29], in which the concept of point-like particle becomes physically meaningless and must be replaced with its best approximation, i.e., a minimal width Gaussian distribution of mass/energy and charge. In fact, the characteristic length scale of this system is given by the matter distribution width $\sqrt{\theta}$. There has been also a growing interest in possible gravitational observable consequences of non-commutativity of space coordinates, specially the behavior of black holes in NC spaces. Solutions of Einstein equations with such smeared sources give new kind of regular black holes in four [30, 31] and higher dimensions [32, 33].

It is worth mentioning that a lower bound for NC parameter θ has been obtained in some papers through study of black holes thermodynamics in NC spaces as $\sqrt{\theta} \sim 10^{-1} l_P$, see e.g., [30, 34, 35]. But according to our knowledge, there is no upper bound on NC parameter obtained in gravitational systems. Generally, in this paper we investigate an upper bound for NC parameter θ , which might make it accessible to measure the minimal length in short range gravity. To determine this bound we use the three aforementioned predictions of GR for the *Schwarzschild* (Sch) and *Reissner-Norström* (RN) backgrounds in NC geometries based on the coordinate coherent state formalism. In the other words, we approximate that the accuracy of our calculations for some typical micro black holes, which can be produced in the early universe, be of order of the accuracy of gravitational measurements, then, we determine a numerical value for upper bound on θ . We have also schematically compared our NC calculations with the GR predictions.

2 Non-commutative geometry in coordinate coherent state formalism

In the original idea of Snyder in [28] there is a minimal length scale $\sqrt{\theta}$ at which the classical concept of smooth spacetime manifold breaks down. From this perspective the θ parameter is a length squared quantity defining the scale where spacetime coordinates become non-commuting (for more study in this formalism see Refs. [36]- [40] and Refs. there in). In the coordinate coherent state formalism, instead of a point-like structure for the matter, it has usually used a “matter droplet” description for the mass with a Gaussian distribution [30]. The starting point is the distributions

$$\rho_M(r) = \frac{M}{(4\pi\theta)^{\frac{3}{2}}} \exp\left(-\frac{r^2}{4\theta}\right), \quad (2.1)$$

$$\rho_Q(r) = \frac{Q}{(4\pi\theta)^{\frac{3}{2}}} \exp\left(-\frac{r^2}{4\theta}\right), \quad (2.2)$$

where θ is the NC parameter in (1.1). For an observer at large distance this smeared density is looks like a small sphere of matter with radius about $\sqrt{\theta}$, so, Birkhoff theorem assures the metric to be Sch and in the presence of charged distribution to be RN. But in the intermediate region the metric is neither Sch, nor RN and can be analytically written in terms of lower incomplete gamma function or error functions as shown bellow. The value of the total mass and charge are given by the integration of this bell-shaped function over the whole space as

$$M_\theta = 4\pi \int r^2 \rho_M(r) dr = M \operatorname{erf}\left[\frac{r}{2\sqrt{\theta}}\right] - \frac{Mr}{\sqrt{\pi\theta}} e^{-\frac{r^2}{4\theta}}, \quad (2.3)$$

$$Q_\theta = Q \operatorname{erf}\left[\frac{r}{2\sqrt{\theta}}\right] + \frac{Qr}{\sqrt{\pi\theta}} e^{-\frac{r^2}{4\theta}}, \quad (2.4)$$

where “erf” is the error function with the following properties

$$\lim_{x \rightarrow \infty} \operatorname{erf}[x] = 1, \quad \lim_{x \rightarrow \infty} \operatorname{erfc}[x] = 0. \quad (2.5)$$

In this paper we study the solutions of Einstein equations described by stationary, spherically symmetric, asymptotically flat metrics which their line element is given by

$$ds^2 = -B(r)dt^2 + \frac{dr^2}{B(r)} + r^2 d\Omega_2^2, \quad (2.6)$$

where for Sch and RN metrics we respectively have

$$B_{Sch}(r) = 1 - \frac{2GM}{r}, \quad B_{RN}(r) = 1 - \frac{2GM}{r} + \frac{Q^2}{r^2}. \quad (2.7)$$

If we insert the mass distribution (2.1) in the Einstein equations of motion, it can be seen that the solution for a Sch black hole which its mass is modified by substituting the mass (2.3), is given by

$$B_{Sch}^{NC}(r) = 1 - \frac{2GM}{r} + \frac{2GM}{r} \operatorname{erfc}\left[\frac{r}{2\sqrt{\theta}}\right] + \frac{2GMe^{-\frac{r^2}{4\theta}}}{\sqrt{\pi\theta}}, \quad (2.8)$$

and in the case of both (2.1) and (2.2), we achieve a modified RN metric

$$B_{RN}^{NC}(r) = 1 - \frac{2GM}{r} + \frac{2GM}{r} \operatorname{erfc}\left[\frac{r}{2\sqrt{\theta}}\right] + \frac{2GM e^{-\frac{r^2}{4\theta}}}{\sqrt{\pi\theta}} + \frac{Q^2 \operatorname{erfc}\left[\frac{r}{2\sqrt{\theta}}\right]^2}{r^2} - \frac{Q^2}{r\sqrt{2\pi\theta}} \left(\operatorname{erfc}\left[\frac{r}{\sqrt{2\theta}}\right] - \operatorname{erfc}\left[\frac{r}{2\sqrt{\theta}}\right] \right) - \frac{Q^2 e^{-\frac{r^2}{4\theta}}}{\sqrt{2\pi\theta}}. \quad (2.9)$$

It must be noticed that in the limit $\frac{r}{\sqrt{\theta}} \rightarrow \infty$ or $\frac{\sqrt{\theta}}{r} \rightarrow 0$, we obtain the metrics described by (2.7) [31]. As we know for a typical gravitational system, such as the sun, the value of the terms including $\frac{2GM}{r}$ in (2.8) are very small even for lowest value of r , which can be the Schwarzschild radius of the gravitational system, so, in the next calculations we can ignore the higher orders without lose of generality. To prove that the last term in (2.8) is very small, we have plotted this term in terms of different values of parameter θ for the schwarzschild radius of the sun, r_o , as shown in Fig. (1). It is easy to check that for larger distances, i.e., $r > r_o$, the value of the peak decreases. Also, we can check this behavior for other gravitational systems but we should pay attention that by increasing the mass, the radius of schwartschild increases, too.

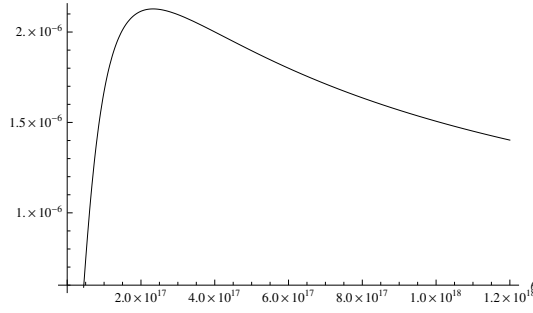


Figure 1: The last term of (2.8).

We have also applied similar consideration for the terms in the second line of relation (2.9). The plots shown in the Figs. (2) are given for the first and the second term, respectively.

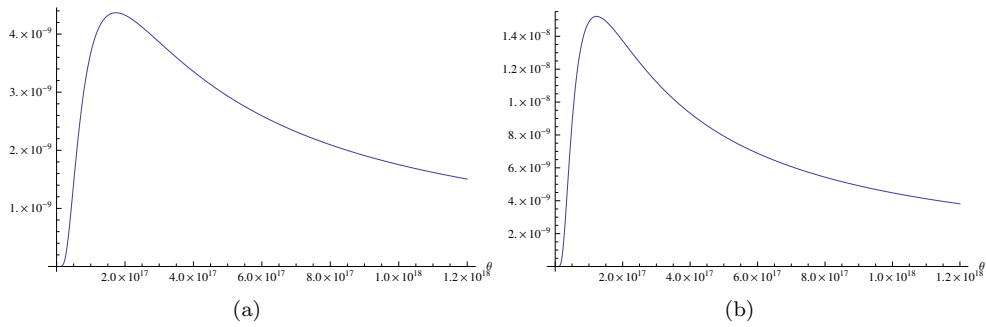


Figure 2: The first and the second terms in line two of (2.9).

In contradiction to the case of Sch solution in GR which has a single horizon, in NC space we have

different possibilities:

- For $\eta = \frac{M}{\sqrt{\theta}} < 1.9$ there is no horizon for (2.8) shown by red solid curve in Fig. (3)
- For $\eta = \frac{M}{\sqrt{\theta}} = 1.9$ there is a degenerate horizon in $x = \frac{r}{\sqrt{\theta}} = 3$ shown by blue curve in Fig. (3).
- For $\eta = \frac{M}{\sqrt{\theta}} > 1.9$ there are two distinct horizons shown by green curve in Fig. (3).

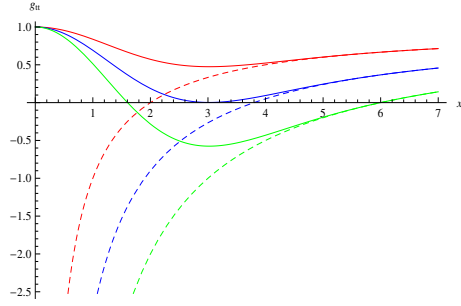


Figure 3: The Schwarzschild metric in commutative (dashed) and non-commutative (solid) spaces for different values of $\frac{M}{\sqrt{\theta}}$.

We have also plotted the tt component of charged solution metric (2.9) in Fig. (4). As seen in the limit $\gamma = \frac{Q}{\sqrt{\theta}} \rightarrow 0$, we obtain the plots for Sch solution in NC space shown in Fig. (3).

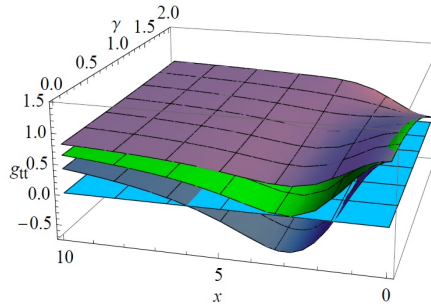


Figure 4: The Reissner-Nordstrom metric in NC space vs. $x = \frac{r}{\sqrt{\theta}}$ and $\gamma = \frac{Q}{\sqrt{\theta}}$ for different values of $\frac{M}{\sqrt{\theta}}$.

2.1 Modified Newton's law

In this subsection, we investigate modification of the Newton's law in coordinate coherent state formalism by using modified metric of Sch geometry. As done in [41], one can obtain first the gravitational field as acceleration of a test particle around the massive object, such as a Sch black hole, and then multiplying by the mass of particle we reproduce the Newton's law of gravity [42]. In this paper we use another approach in which we first calculate the energy of particle and then its derivative gives the Newton's law. The energy of a test particle of mass m moving with four-velocity u^μ in a curved space with non-rotating,

spherical symmetry is

$$E = mt_\mu u^\mu = mg_{\mu\nu} t^\nu u^\mu = mg_{00} t^0 u^0 = -mB(r) \frac{dt}{ds}, \quad (2.10)$$

where t^μ is a time-like killing vector $t^\mu = (1, 0, 0, 0)$. When the particle is at distance r , by substituting $dr = d\Omega = 0$ in the metric (2.6) we have $ds^2 = -B(r)dt^2$, thus the energy becomes

$$E = m\sqrt{-B(r)}. \quad (2.11)$$

Now by differentiating with respect to the r , we obtain the gravitational force on the test particle as

$$F = m \frac{B'(r)}{2\sqrt{-B(r)}}. \quad (2.12)$$

Substituting $B(r)$ from the relations (2.8) and (2.9) in (2.12), the gravitational force for the Sch and RN metrics are given by

$$F_{Sch}^{NC} = \frac{GmM}{r^2} \left(1 - \frac{r^3 e^{-\frac{r^2}{4\theta}}}{2\sqrt{\pi}\theta^{3/2}} - \frac{r e^{-\frac{r^2}{4\theta}}}{\sqrt{\pi}\theta} - \operatorname{erfc} \left[\frac{r}{2\sqrt{\theta}} \right] \right), \quad (2.13)$$

$$\begin{aligned} F_{RN}^{NC} = F_{Sch}^{NC} - \frac{mQ^2}{r^3} & \left(1 - \frac{r^4 e^{-\frac{r^2}{4\theta}}}{4\sqrt{2}\pi\theta^2} + \frac{r^2 e^{-\frac{r^2}{2\theta}}}{2\pi\theta} - \frac{r^2 e^{-\frac{r^2}{4\theta}}}{2\sqrt{2}\pi\theta} \right. \\ & \left. - \frac{r e^{-\frac{r^2}{2\theta}}}{\sqrt{\pi}\theta} \operatorname{erfc} \left[\frac{r}{2\sqrt{\theta}} \right] + \frac{r}{2\sqrt{2}\pi\theta} \operatorname{erfc} \left[\frac{r}{2\sqrt{\theta}} \right] + \operatorname{erfc} \left[\frac{r}{2\sqrt{\theta}} \right]^2 - \frac{r}{2\sqrt{2}\pi\theta} \operatorname{erfc} \left[\frac{r}{\sqrt{2\theta}} \right] \right), \end{aligned} \quad (2.14)$$

where in the limit $\frac{\sqrt{\theta}}{r} \rightarrow 0$ they lead to general Newton's law $F = \frac{GMm}{r^2}$. We have neglected the relativistic term $[-B(r)]^{-1/2}$, since this term produce higher order corrections in GM/r and Q^2/r^2 . One can use the relations (2.13) and (2.14) to study the gravitational atoms formed by black holes which are candidates for Dark matter.

3 Gravitational red-shift

When the light moves upwards against gravitational field, it loses some of its energy, so it undergoes a red-shift [1, 5]. Indeed, light from high frequency (short wavelength) leads to a light with low frequency (long wavelength), and in fact, there is a shift in the spectral lines of light due to gravity by

$$z = \frac{\omega_2 - \omega_1}{\omega_1}, \quad (3.1)$$

which is known as gravitational red-shift of light and is a direct consequence of Einstein General relativity theory. Now suppose that light was emitted from radius r_1 and received at r_2 , so, in the case of general metric given in (2.6) the value by which the light be red-shifted is [5]

$$z = \frac{\omega_2}{\omega_1} - 1 = \sqrt{\frac{B(r_1)}{B(r_2)}} - 1, \quad (3.2)$$

where ω_2 and ω_1 are the frequency recieved by the observer and the frequency emitted by the source, respectively. Substituting the fuctions in (2.7) in (3.2) we obtain the gravitational red-shift for the Sch and RN black holes in GR, respectively,

$$z = \sqrt{\left(1 - \frac{2GM}{r_1}\right) \left(1 - \frac{2GM}{r_2}\right)^{-1}} - 1, \quad z = \sqrt{\left(1 - \frac{2GM}{r_1} + \frac{Q^2}{r_1^2}\right) \left(1 - \frac{2GM}{r_2} + \frac{Q^2}{r_2^2}\right)^{-1}} - 1. \quad (3.3)$$

3.1 Gravitational red-shift in non-commutative space

In this subsection we first study the behavior of gravitational red-shift factor for the Sch and RN backgrounds and then, we find upper bounds for the NC parameter θ by comparing the results with the accuracy of the measurements. The red-shift for Sch metric measured by an asymptotic observer, $r_2 \rightarrow \infty$, is given by substituting the component (2.8) in the relation (3.2)

$$z = \left(1 - \frac{2GM}{r_1} + \frac{2GM \operatorname{erfc}\left[\frac{r_1}{2\sqrt{\theta}}\right]}{r_1} + \frac{2GM e^{-\frac{r_1^2}{4\theta}}}{\sqrt{\pi\theta}}\right)^{\frac{1}{2}} - 1, \quad (3.4)$$

and for the RN metric by inserting (2.9) in the relation (3.2) we have

$$\begin{aligned} z = & \left[1 - \frac{2GM}{r_1} + \frac{2GM \operatorname{erfc}\left[\frac{r_1}{2\sqrt{\theta}}\right]}{r_1} + \frac{2GM e^{-\frac{r_1^2}{4\theta}}}{\sqrt{\pi\theta}} + \frac{Q^2 \operatorname{erfc}\left[\frac{r_1}{2\sqrt{\theta}}\right]^2}{r_1^2}\right. \\ & \left. - \frac{Q^2}{r_1 \sqrt{2\pi\theta}} \left(\operatorname{erfc}\left[\frac{r_1}{\sqrt{2\theta}}\right] - \operatorname{erfc}\left[\frac{r_1}{2\sqrt{\theta}}\right]\right) - \frac{Q^2 e^{-\frac{r_1^2}{4\theta}}}{\sqrt{2\pi\theta}}\right]^{\frac{1}{2}} - 1, \end{aligned} \quad (3.5)$$

where again in the limit $\frac{\sqrt{\theta}}{r} \rightarrow 0$, they lead to the GR red-shifts (3.3). We have plotted the red-shifts for both the Sch (blue curve) and RN (red curve) metrics in non-commutative and GR background (black and green curves) in Fig. (5) in terms of the scaled radial coordinate $x = \frac{r_1}{\sqrt{\theta}}$. As expected for far regions from the gravitational system all of them get to zero and there is no shift in the light wavelength. It can be also seen that in contrast to GR predictions, there is a finite maximum for the redshift value and this extremum occurs at $x = 3$ (of course for the RN not exactly at $x = 3$), which is consistent with the extremal limit, $\eta = 1.9$, illustrated in Fig. (3). On the other hand, this extremum value happens at the degenerate horizon. Comparing the plot of the Sch and RN Fig. (5), we can infer that the extremum value has decreased for the RN background metric relative to Sch's one.

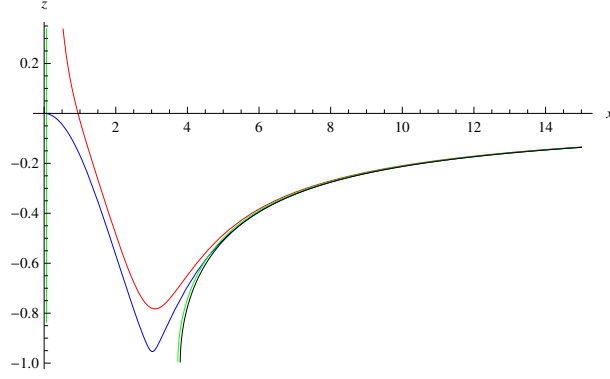


Figure 5: The red-shift of non-commutative Sch (blue curve) and RN (red curve) metric vs. $x = \frac{r_1}{\sqrt{\theta}}$ for $\eta = \frac{M}{\sqrt{\theta}} = 1.9$ and $\gamma = \frac{Q}{\sqrt{\theta}} = 0.5$. The green and black curves are the Sch and RN metrics in GR, respectively.

4 Gravitational deflection of light

One of the other interesting predictions and early monumental verifications of GR is the deflection of light caused by gravity which also known as gravitational lensing. When the light passes close to a massive object, such as a supernova or a black hole, it is deflected from its straight path which is given by the following relation [5]

$$\Delta\phi = 2 \int_{r_o}^{\infty} \frac{1}{r\sqrt{B(r)}} \left(\frac{r^2}{r_o^2} \frac{B(r_o)}{B(r)} - 1 \right)^{-\frac{1}{2}} dr - \pi, \quad (4.1)$$

where r_o is the closest distance to the massive object. Calculating the integration yields to the following expressions for the Sch and RN metrics, in commutative space:

$$\Delta\phi_{Sch} = \frac{4GM}{r_o}, \quad \Delta\phi_{RN} = \frac{4GM}{r_o} - \frac{3\pi Q^2}{4r_o^2}. \quad (4.2)$$

4.1 Deflection of light in non-commutative spaces

This part of the work is devoted to the study of deflection of light (light bending) in the NC spaces. By substituting the metric (2.8) in the relation (4.1) we have

$$\begin{aligned} \Delta\phi = & 2 \int_{r_o}^{\infty} \left[\frac{1}{r\sqrt{\frac{r^2}{r_o^2} - 1}} - \frac{GM}{\left(\frac{r^2}{r_o^2} - 1\right)^{3/2}r_o^2} + \frac{GMr}{\left(\frac{r^2}{r_o^2} - 1\right)^{3/2}r_o^3} + \frac{GM}{r^2\sqrt{\frac{r^2}{r_o^2} - 1}} \right. \\ & + \frac{GM\text{erfc}\left(\frac{r}{2\sqrt{\theta}}\right)}{\left(\frac{r^2}{r_o^2} - 1\right)^{3/2}r_o^2} - \frac{GMr\text{erfc}\left(\frac{r_o}{2\sqrt{\theta}}\right)}{\left(\frac{r^2}{r_o^2} - 1\right)^{3/2}r_o^3} - \frac{GM\text{erfc}\left(\frac{r}{2\sqrt{\theta}}\right)}{r^2\sqrt{\frac{r^2}{r_o^2} - 1}} + \frac{GMre^{-\frac{r^2}{4\theta}}}{\sqrt{\pi}\sqrt{\theta}\left(\frac{r^2}{r_o^2} - 1\right)^{3/2}r_o^2} \\ & \left. - \frac{GMre^{-\frac{r_o^2}{4\theta}}}{\sqrt{\pi}\sqrt{\theta}\left(\frac{r^2}{r_o^2} - 1\right)^{3/2}r_o^2} - \frac{GMe^{-\frac{r^2}{4\theta}}}{\sqrt{\pi}\sqrt{\theta}r\sqrt{\frac{r^2}{r_o^2} - 1}} \right] dr - \pi, \end{aligned} \quad (4.3)$$

After the integration we obtain the deflection of light caused by the Sch metric as follows

$$\Delta\phi_{Sch}^{NC} = \frac{4GM}{r_o} - \frac{4GMe^{-\frac{r_o^2}{4\theta}}}{r_o} - \frac{GMr_o e^{-\frac{r_o^2}{4\theta}}}{\theta}. \quad (4.4)$$

In the limit $\frac{\sqrt{\theta}}{r} \rightarrow 0$ this relation goes to the GR prediction (4.2). In the case of RN metric described by (2.9), the integral (4.1) leads to

$$\begin{aligned} \Delta\phi = & -\pi + 2 \int_{r_o}^{\infty} dr \left[\frac{1}{r\sqrt{\frac{r^2}{r_o^2} - 1}} - \frac{GM}{\left(\frac{r^2}{r_o^2} - 1\right)^{3/2} r_o^2} + \frac{GM r}{\left(\frac{r^2}{r_o^2} - 1\right)^{3/2} r_o^3} + \frac{GM}{r^2 \sqrt{\frac{r^2}{r_o^2} - 1}} - \frac{GM \text{erfc}\left(\frac{r}{2\sqrt{\theta}}\right)}{\left(\frac{r^2}{r_o^2} - 1\right)^{3/2} r_o^2} \right. \\ & + \frac{GM r \text{erfc}\left(\frac{r_o}{2\sqrt{\theta}}\right)}{\left(\frac{r^2}{r_o^2} - 1\right)^{3/2} r_o^3} - \frac{GM \text{erfc}\left(\frac{r}{2\sqrt{\theta}}\right)}{r^2 \sqrt{\frac{r^2}{r_o^2} - 1}} + \frac{GM r e^{-\frac{r^2}{4\theta}}}{\sqrt{\pi} \sqrt{\theta} \left(\frac{r^2}{r_o^2} - 1\right)^{3/2} r_o^2} - \frac{GM r e^{-\frac{r_o^2}{4\theta}}}{\sqrt{\pi} \sqrt{\theta} \left(\frac{r^2}{r_o^2} - 1\right)^{3/2} r_o^2} \\ & - \frac{GM e^{-\frac{r^2}{4\theta}}}{\sqrt{\pi} \sqrt{\theta} r \sqrt{\frac{r^2}{r_o^2} - 1}} + \frac{Q^2 \text{erf}\left(\frac{r}{2\sqrt{\theta}}\right)}{2\sqrt{2\pi} r_o^2 \sqrt{\theta} \left(\frac{r^2}{r_o^2} - 1\right)^{3/2}} - \frac{Q^2 \text{erf}\left(\frac{r}{2\sqrt{\theta}}\right)}{2\sqrt{2\pi} r_o^2 \sqrt{\theta} \left(\frac{r^2}{r_o^2} - 1\right)^{3/2}} - \frac{Q^2 r e^{-\frac{r^2}{4\theta}}}{2\sqrt{2\pi} r_o^2 \sqrt{\theta} \left(\frac{r^2}{r_o^2} - 1\right)^{3/2}} \\ & + \frac{Q^2 r e^{-\frac{r_o^2}{4\theta}}}{2\sqrt{2\pi} r_o^2 \sqrt{\theta} \left(\frac{r^2}{r_o^2} - 1\right)^{3/2}} + \frac{Q^2 r \text{erf}\left(\frac{r_o}{2\sqrt{\theta}}\right)}{2\sqrt{2\pi} r_o^3 \sqrt{\theta} \left(\frac{r^2}{r_o^2} - 1\right)^{3/2}} - \frac{Q^2 r \text{erf}\left(\frac{r_o}{2\sqrt{\theta}}\right)}{2\sqrt{2\pi} r_o^3 \sqrt{\theta} \left(\frac{r^2}{r_o^2} - 1\right)^{3/2}} + \frac{Q^2 \text{erfc}\left(\frac{r}{2\sqrt{\theta}}\right)^2}{2r_o^2 r \left(\frac{r^2}{r_o^2} - 1\right)^{3/2}} \\ & - \frac{Q^2 \text{erfc}\left(\frac{r}{2\sqrt{\theta}}\right)}{r_o^2 r \left(\frac{r^2}{r_o^2} - 1\right)^{3/2}} + \frac{Q^2 \text{erfc}\left(\frac{r}{2\sqrt{\theta}}\right)}{r^3 \sqrt{\frac{r^2}{r_o^2} - 1}} - \frac{Q^2 \text{erfc}\left(\frac{r}{2\sqrt{\theta}}\right)^2}{2r^3 \sqrt{\frac{r^2}{r_o^2} - 1}} + \frac{Q^2 r \text{erfc}\left(\frac{r_o}{2\sqrt{\theta}}\right)}{r_o^4 \left(\frac{r^2}{r_o^2} - 1\right)^{3/2}} - \frac{Q^2 r \text{erfc}\left(\frac{r_o}{2\sqrt{\theta}}\right)}{2r_o^4 \left(\frac{r^2}{r_o^2} - 1\right)^{3/2}} \Big]. \quad (4.5) \end{aligned}$$

In this relation, the last six terms can not be integrated directly. But, by numerical integration we can see that four terms of them are exactly opposit to each other and two terms have very small values, so, we neglect them in our calculation. Also for the remaining terms that have direct integration, for some typical values of Q , M , and θ , the result of integrations are very small values in comparison with the other ones, therefore, the final result is

$$\Delta\phi = \frac{4GM}{r_o} - \frac{3\pi Q^2}{4r_o^2} - \frac{4GM e^{-\frac{r_o^2}{4\theta}}}{r_o} - \frac{GM r_o e^{-\frac{r_o^2}{4\theta}}}{\theta} + \frac{r_o Q^2 e^{-\frac{r_o^2}{4\theta}}}{2\sqrt{2\pi} \theta^{3/2}}. \quad (4.6)$$

Again, we can see that in the limit $\frac{\sqrt{\theta}}{r} \rightarrow 0$, this relation goes to (4.2) i.e., the RN background in commutative space. Now, in order to show the differences between commutative and non-commutative geometries we plot the deflection relations. For example, in Fig. (6) we have plotted the relations (4.2) and (4.4) for the Sch and Sch metrics. The figure has been plotted for $\eta = \frac{M}{\sqrt{\theta}} = 1.9$ and the maximum of the red curve is located around $x = \frac{r_o}{\sqrt{\theta}} = 3$, which was the location of the degenerate horizon as mentioned in previous discussions. As it is observed, unlike commutative space, there is a finite deflection for light in NC geometry at the horizon and lower distances.

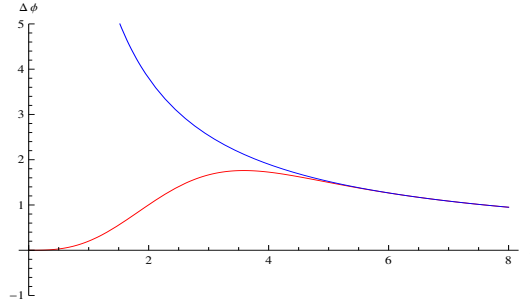


Figure 6: The Schwarzschild deflection for GR prediction (blue curve) and NC geometry (red curve).

We have also plotted the deflection of light which occurs in the vicinity of an RN metric with charge $\gamma = \frac{Q}{\sqrt{\theta}} = 0.5$ in Fig. (7). The blue curve is for GR given by (4.2) and the red one shows the results of RN metric in NC spaces as given by (4.6). Again it is seen that, there is a finite deflection for the light around the local event horizon. It is worth to mention that the results of both Sch and RN metrics coincide to the commutative case in the limit $\frac{r}{\sqrt{\theta}} \rightarrow 0$.

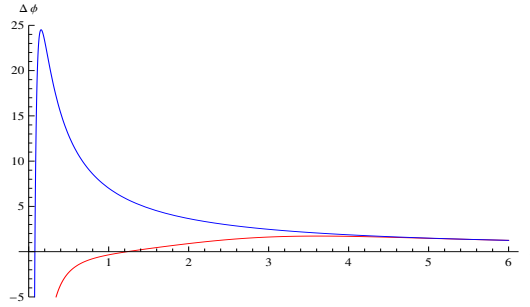


Figure 7: The RN deflection for GR prediction (blue curve) and NC geometry (red curve).

5 Gravitational time delay

Gravitational time dilation is an actual difference of elapsed time between two events as measured by observers differently situated from a massive gravitational object. Since light has an effective mass, it is affected by gravity, so, it follows a curved trajectory or a curved path when exposed to gravitational force. However, this is not actually what happens because gravity curves spacetime and light bends because it has to travel through that curved space-time. Since high gravity attracts things more towards itself (lensing), light bends more in a region of high gravity. We also know that a straight path is always shorter than a curved path in terms of distance traversed. So, a light ray that bends more has to travel a longer distance to reach the destination and therefore takes more time than a light ray that bends lesser. Einstein originally predicted this effect in his theory of relativity and it has since been confirmed by tests of GR. This phenomena was discovered and observed for the first time in 1964 by Shapiro [44], which it is also called Shapiro time delay. In GR, objects cause space-time curvature and the motion of objects is

also affected by space-time geometry.

Suppose that the light travels from $r = r_1$ to $r = r_2$, then the time delay is given by

$$\Delta t_{max} = 2 \left(t(r_o, r_1) + t(r_o, r_2) - \sqrt{r_o - r_1} - \sqrt{r_o - r_2} \right), \quad (5.1)$$

where $t(r_o, r)$ is

$$t(r_o, r) = \int_{r_o}^r \frac{1}{B(r)} \left(1 - \frac{r_o^2}{r^2} \frac{B(r)}{B(r_o)} \right)^{-\frac{1}{2}} dr, \quad (5.2)$$

and r_o is the distance of closest approach to the typical gravitational system (a massive object). By substituting (2.7) in (5.2) and then the result in (5.1), the time delations for the light traveling from the source to target in commutative geometry for Sch and RN black holes are

$$\Delta t_{max}^{Sch} = 4MG \left(1 + \ln \frac{4r_1 r_2}{r_o^2} \right), \quad \Delta t_{max}^{RN} = 4MG \left(1 + \ln \frac{4r_1 r_2}{r_o^2} \right) - 3 \frac{Q^2 \pi}{r_o}, \quad (5.3)$$

where r_o is the event horizon of the massive object and r_1, r_2 are distances of the source and target to it, respectively.

5.1 Shapiro time delay in non-commutative space

In order to study the Shapiro time delay in NC geometries we will evaluate the integral (5.2) for the Sch (2.8) and RN (2.9) metrics, separately. After integrating we arrive at the following expression for Sch background

$$\begin{aligned} t(r_o, r) = & 2GM \ln \left(\frac{\sqrt{r^2 - r_o^2} + r}{r_o} \right) + \sqrt{r^2 - r_o^2} + GM \sqrt{\frac{r_o - r}{r_o + r}} - \frac{r_o^2 G M e^{-\frac{r_o^2}{4\theta}} \operatorname{erf} \left(\frac{\sqrt{r^2 - r_o^2}}{2\sqrt{\theta}} \right)}{2\theta} \\ & - \frac{r_o G M \operatorname{erf} \left(\frac{r_o}{2\sqrt{\theta}} \right)}{r \sqrt{1 - \frac{r_o^2}{r^2}}} + \frac{G M \operatorname{erf} \left(\frac{r}{2\sqrt{\theta}} \right)}{\sqrt{1 - \frac{r_o^2}{r^2}}} - 3 G M e^{-\frac{r_o^2}{4\theta}} \operatorname{erf} \left(\frac{\sqrt{r^2 - r_o^2}}{2\sqrt{\theta}} \right) + \frac{r_o^2 G M e^{-\frac{r_o^2}{4\theta}}}{\sqrt{\pi} \sqrt{\theta} r \sqrt{1 - \frac{r_o^2}{r^2}}} \\ & - \frac{r_o^2 G M e^{-\frac{r_o^2}{4\theta}}}{\sqrt{\pi} \sqrt{\theta} r \sqrt{1 - \frac{r_o^2}{r^2}}} - \int_{r_o}^r \frac{2 G M \operatorname{erfc} \left(\frac{r}{2\sqrt{\theta}} \right)}{r \sqrt{1 - \frac{r_o^2}{r^2}}} dr, \end{aligned} \quad (5.4)$$

where the first three terms come from GR and the rest terms are corrections due to non-commutativity of space-time, so the time delation from (5.1) is given by

$$\begin{aligned}
\Delta t_{max}^{NC-Sch} = & \Delta t_{max}^{Sch} - \frac{r_o^2 G M e^{-\frac{r_o^2}{4\theta}} \operatorname{erf}\left(\frac{\sqrt{r_1^2 - r_o^2}}{2\sqrt{\theta}}\right)}{\theta} - \frac{r_o^2 G M e^{-\frac{r_o^2}{4\theta}} \operatorname{erf}\left(\frac{\sqrt{r_2^2 - r_o^2}}{2\sqrt{\theta}}\right)}{\theta} \\
& - \frac{2r_o G M \operatorname{erf}\left(\frac{r_o}{2\sqrt{\theta}}\right)}{r_1 \sqrt{1 - \frac{r_o^2}{r_1^2}}} - \frac{2r_o G M \operatorname{erf}\left(\frac{r_o}{2\sqrt{\theta}}\right)}{r_2 \sqrt{1 - \frac{r_o^2}{r_2^2}}} - 6G M e^{-\frac{r_o^2}{4\theta}} \operatorname{erf}\left(\frac{\sqrt{r_1^2 - r_o^2}}{2\sqrt{\theta}}\right) \\
& - 6G M e^{-\frac{r_o^2}{4\theta}} \operatorname{erf}\left(\frac{\sqrt{r_2^2 - r_o^2}}{2\sqrt{\theta}}\right) + \frac{2G M \operatorname{erf}\left(\frac{r_1}{2\sqrt{\theta}}\right)}{\sqrt{1 - \frac{r_o^2}{r_1^2}}} + \frac{2G M \operatorname{erf}\left(\frac{r_2}{2\sqrt{\theta}}\right)}{\sqrt{1 - \frac{r_o^2}{r_2^2}}} + \frac{2r_o^2 G M e^{-\frac{r_o^2}{4\theta}}}{\sqrt{\pi} \sqrt{\theta} r_1 \sqrt{1 - \frac{r_o^2}{r_1^2}}} \\
& - \frac{2r_o^2 G M e^{-\frac{r_o^2}{4\theta}}}{\sqrt{\pi} \sqrt{\theta} r_1 \sqrt{1 - \frac{r_o^2}{r_1^2}}} + \frac{2r_o^2 G M e^{-\frac{r_o^2}{4\theta}}}{\sqrt{\pi} \sqrt{\theta} r_2 \sqrt{1 - \frac{r_o^2}{r_2^2}}} - \frac{2r_o^2 G M e^{-\frac{r_o^2}{4\theta}}}{\sqrt{\pi} \sqrt{\theta} r_2 \sqrt{1 - \frac{r_o^2}{r_2^2}}} \\
& - 4 \int_{r_o}^{r_1} \frac{2G M \operatorname{erfc}\left(\frac{r}{2\sqrt{\theta}}\right)}{r \sqrt{1 - \frac{r_o^2}{r^2}}} dr - 4 \int_{r_o}^{r_2} \frac{2G M \operatorname{erfc}\left(\frac{r}{2\sqrt{\theta}}\right)}{r \sqrt{1 - \frac{r_o^2}{r^2}}} dr, \tag{5.5}
\end{aligned}$$

where the first term given in (5.3) shows the GR contribution and is equal to $240 (\mu s)$ or $72000 (m)$ for a solar system in which M , r_o , r_1 , and r_2 are the mass and radius of the sun, distances of earth and mercury from the sun, respectively. One can check that (5.5) goes to GR prediction in the limit $\frac{r}{\sqrt{\theta}} \rightarrow \infty$. Also, for any value of θ , the contribution of the last two terms that are given by integrals, are negligible in comparsion with the other terms. In addition, for any gravitational systems like sun or other black holes, we have numerically checked that the contribution of some of terms are very small in comparsion with the others. Therefore the expression reduces to

$$\Delta t_{max}^{NC-Sch} = \Delta t_{max}^{Sch} - \left(\frac{r_o^2 G M e^{-\frac{r_o^2}{4\theta}}}{\theta} + 6G M e^{-\frac{r_o^2}{4\theta}} \right) \left[\operatorname{erf}\left(\frac{r_1}{2\sqrt{\theta}}\right) + \operatorname{erf}\left(\frac{r_2}{2\sqrt{\theta}}\right) \right], \tag{5.6}$$

where we have ignored from r_o in comparsion with r_1 and r_2 . As we know, r_1 and r_2 are distances from the center of typical gravitational system, to two points outside of it. On the other hand, we expect that the value of θ to be much smaller than r_1 and r_2 . So, by this assumption we have checked that the error functions in (5.6) go to unit value. Therefore the final expression is as follow

$$\Delta t_{max}^{NC-Sch} = \Delta t_{max}^{Sch} - 2 \frac{r_o^2 G M e^{-\frac{r_o^2}{4\theta}}}{\theta} - 12G M e^{-\frac{r_o^2}{4\theta}}. \tag{5.7}$$

For the RN background, the calculation method is the same as the previous one. So, we refrain from providing details and only provide the final expression

$$\Delta t_{max}^{NC-RN} = \Delta t_{max}^{RN} - 12G M e^{\frac{r_o^2}{4\theta}} - \frac{2r_o^2 G M e^{-\frac{r_o^2}{4\theta}}}{\theta} - \frac{2r_o^2 Q^2 e^{-\frac{r_o^2}{4\theta}}}{\sqrt{2\pi} \theta^{3/2}} + \frac{4Q^2 e^{-\frac{r_o^2}{2\theta}}}{\sqrt{2\pi} \theta}. \tag{5.8}$$

In Fig. (8) We have plotted both GR and NC predictions of dimensionless parameter $\xi = \frac{\Delta t_{max}}{r_o}$ instead of time delay for both Sch and RN metrics. As seen in both figures, the predictions of GR and NC for

large distances become consistent while in the vicinity of degenerate horizon at $x = \frac{r}{\sqrt{\theta}} = 3$ the difference is obvious.

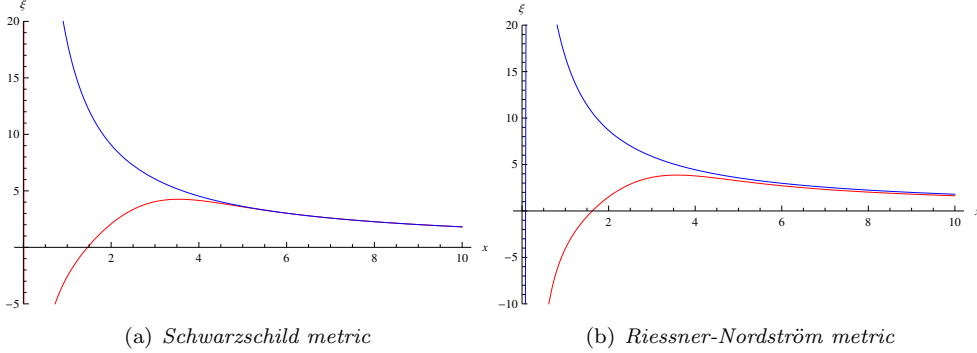


Figure 8: maximum time delay for GR (blue curves) and NC (red curves) for $\eta = 1.9$ and $\gamma = \frac{Q}{\sqrt{\theta}} = 0.5$.

6 Upper bound on θ

An interesting point is that by comparing the corrections due to non-commutativity of spaces on different gravitational measurements, discussed in this paper, with their accuracies of measurements, one can impose some bounds on the value of the NC parameter θ . It is worth mentioning that these bounds are calculated for micro black holes which have different masses up to moon's mass. Micro black holes can be created in the early universe and survive until now [43].

For gravitational red shift the most accurate measurement is from Gravity Probe A in 1976 [45]. This accuracy was obtained for a satellite at an altitude of $10^7 m$. By expanding (3.2) we can separate GR term from NC correction terms as follows

$$z_{NC} = z_{GR} \left[1 + \left| \frac{z_{GR} + 1}{z_{GR}} \right| \left(\frac{GM \operatorname{erfc} \left[\frac{r_1}{2\sqrt{\theta}} \right]}{\left(1 - \frac{2GM}{r_1} \right) r_1} + \frac{GM e^{-\frac{r_1^2}{4\theta}}}{\left(1 - \frac{2GM}{r_1} \right) \sqrt{\pi\theta}} \right) \right]. \quad (6.1)$$

The NC correction term should be smaller than the accuracy of measurements which is 7.0×10^{-5} , so, we have

$$\left| \frac{z_{GR} + 1}{z_{GR}} \right| \left(\frac{GM \operatorname{erfc} \left[\frac{r_1}{2\sqrt{\theta}} \right]}{\left(1 - \frac{2GM}{r_1} \right) r_1} + \frac{GM e^{-\frac{r_1^2}{4\theta}}}{\left(1 - \frac{2GM}{r_1} \right) \sqrt{\pi\theta}} \right) \leq 7.0 \times 10^{-5}, \quad (6.2)$$

where z_{GR} is given in Eq. (3.3). Due to complexity of the error function and the presence of an exponential term, solving this inequality is a very difficult task or may be almost impossible, but instead, we have plotted both sides and then find the value of θ in the intersecting point as depicted in Fig. (9). In plotting the figure we have used the mass and radius of a typical micro black hole, $MG \sim 5 \times 10^{-4} (m)$ and $r_1 \sim 1.5 \times 10^{-3} (m)$. Therefore, according to the plot we obtain the upper bound as

$$\alpha \geq 6.6 \Rightarrow \frac{1.5 \times 10^{-3}}{\sqrt{\theta}} \geq 6.6 \Rightarrow \sqrt{\theta} \leq 2 \times 10^{-4} (m). \quad (6.3)$$

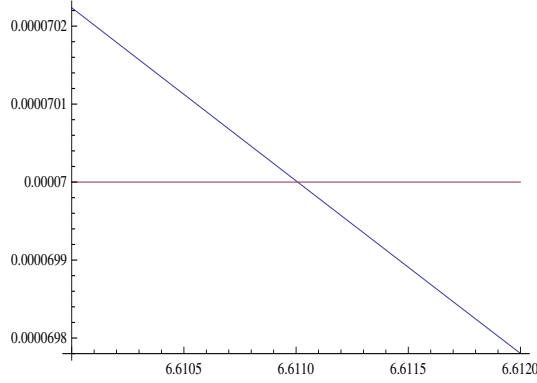


Figure 9: Numerical comparison for red-shift (6.2), the horizontal axis is $\frac{r_1}{\sqrt{\theta}}$

The accuracy 7×10^{-5} is for sun's red shift measurement, but we can convince our selves using this value, because the upper bound is not highly sensitive to the accuracy of measurements which can be easily checked. For instance, if we use the accuracies range from 10^{-2} to 10^{-11} , the value of the upper bound obtained from (6.2) does not change appreciably. This is in fact the case for other upper bound which will be obtained subsequently.

In the case of deflection of light a number of measurements have been made in succeeding years, but there was no significant improvement until the advent of very-long-baseline interferometry (VLBI) [9,10]. VLBI based on the interferometer implication in which there are different radio telescopes situated at distant locations and are utilized simultaneously. This technique creates a virtual radio telescope with a far larger baseline. VLBI uses a geometric method to measure the arrival time of radio waves from an astronomical source between different telescopes. For deflection of light, this project achieved an accuracy of 3×10^{-4} ; Thus, according to the NC definition in (4.4), we should have

$$\frac{|\delta\Delta\phi|}{\Delta\phi_{GR}} \leq 3 \times 10^{-4}, \quad (6.4)$$

where $\delta\Delta\phi = \Delta\phi_{NC} - \Delta\phi_{GR}$. Now, using $r_o \sim 1.5 \times 10^{-3}(m)$ and $GM \sim 5 \times 10^{-4}(m)$ for a micro black hole, we have

$$\frac{r_o}{4GM} \left(\frac{4GM e^{-\frac{r_o^2}{4\theta}}}{r_o} + \frac{GM r_o e^{-\frac{r_o^2}{4\theta}}}{\theta} \right) \leq 3 \times 10^{-4} \Rightarrow \sqrt{\theta} \leq 2.3 \times 10^{-4}(m). \quad (6.5)$$

For the time delay, the best measurement of time delay with high accuracy was obtained by the Cassini spacecraft [46] for time traveling of radio waves from earth to the spacecraft. This accuracy has the absolute value 2.3×10^{-5} , so from the GR time delay in (5.7) we should have

$$\left| \frac{\delta t_{max}^{NC-Sch}}{\Delta t_{max}^{Sch}} \right| \leq 2.3 \times 10^{-5} \Rightarrow \sqrt{\theta} \leq 2.2 \times 10^{-4}(m), \quad (6.6)$$

where $\delta t_{max}^{NC-Sch} = -\frac{2r_o^2 GM e^{-\frac{r_o^2}{4\theta}}}{\theta} - 12GM e^{-\frac{r_o^2}{4\theta}}$. It must be noticed that if we use another accuracies from 10^{-2} to 10^{-11} instead of the above accuracies, the value of the upper bound does not have a considerable difference.

7 Conclusion

In this paper we studied the three most important predictions of Einsteins general relativity in non-commutative spaces. We have obtained the metrics of Sch and RN by using some Gaussian distributions of the mass and charge, as physical parameters of these black holes in NC space, in coordinate coherent state formalism. In contrast to general metrics which have an event horizon for each none-zero value of mass, we showed that in non-commutative spaces, the existence of a horizon was tightly depend on the ratios $\frac{M}{\sqrt{\theta}}$ and $\frac{Q}{\sqrt{\theta}}$. Though we have only an event horizon in the Sch metric, but in this formalism it is possible to have two different horizon for which $B(r)$ vanishes.

We have also obtained exact expressions for the gravitational red-shift in both geometries as a function of r and θ represented by (3.4) and (3.5). As an important result which has been depicted in Fig. (5), in spite of GR in which the red-shift factor does not have a finite value, in NC case we arrived to a maximum value that light might be shifted to the red wavelength. It could even be seen from the figure that for the charged solution this value suppressed near the local degenerate horizon.

In addition we have calculated the value of deflection of light (gravitational lensing) in the framework of NC spaces which is different from GR prediction, that is, there is a maximum value for deflection of light near the horizon in NC solutions shown in Figs. (6) and (7). The third issue discussed in this paper is the gravitational time delay in a NC space. As is obvious from the figures, for all of the predictions the results of NC coincide with the one of commutative case for large values of $x = \frac{r}{\sqrt{\theta}}$ while the differences were appeared in locations around the degenerate horizon at $x = 3$.

Another interesting result is that we have found an upper bound for NC parameter θ using the accuracy of gravitational measurements. The results are summarized in Tab. (1). Though we have used the accuracies obtained from solar systems, but it must be noticed that if we use other accuracies, range from 10^{-2} to 10^{-11} , the value of the upper bounds does not change considerably.

experiment	upper bound (m)
red-shift	$\sqrt{\theta} \leq 2.2 \times 10^{-4}$
deflection	$\sqrt{\theta} \leq 2.3 \times 10^{-4}$
time delay	$\sqrt{\theta} \leq 2.2 \times 10^{-4}$

Table 1: Upper bounds on θ for different tests of GR

These results were obtained for some typical micro black holes which their masses are near the mass of the moon. Additional notable feature of these calculations is that the range of the NC parameter given in Tab (1) is of the order of the scale that some experiments test the gravity at short distances [47, 48]. These calculations can be generalized to higher dimensional theories of gravity as future studies.

References

- [1] B. Schutz, “A first course in General Relativity,” (Cambridge UK: Cambridge University Press, 2009).
- [2] C. W. Misner, K. S. Thorne and J. A. Wheeler, “Gravitation,” San Francisco 1973, 1279p
- [3] A. S. Eddington, “Report on the Relativity Theory of Gravitation”, (Fleetwood Press, London UK, 1918)
- [4] J. Earman and C. Glymour, “Studies in History and Philosophy of Science,” 11 175-214, (1980).
- [5] S. Weinberg, “Gravitation and Cosmology: Principles and Applications of the General Theory of Relativity,” (New York, NY: John Wiley and Sons, 1972).
- [6] S. Carroll, “Spacetime and Geometry: An Introduction to General Relativity”, (Addison Wesley 2004).
- [7] F. W. Dyson, A. S. Eddington and C. Davidson, “A Determination of the Deflection of Light by the Sun’s Gravitational Field, from Observations Made at the Total Eclipse of May 29, 1919,” Phil. Trans. Roy. Soc. Lond. A **220**, 291 (1920).
- [8] P. J. E. Peebles, “Probing general relativity on the scales of cosmology,” astro-ph/0410284.
- [9] E. B. Fomalont and R. A. Sramek, “Measurements of the Solar Gravitational Deflection of Radio Waves in Agreement with General Relativity,” Phys. Rev. Lett. **36**, 1475 (1976).
- [10] E. Fomalont, S. Kopeikin, G. Lanyi and J. Benson, “Progress in Measurements of the Gravitational Bending of Radio Waves Using the VLBA,” Astrophys. J. **699**, 1395 (2009)
- [11] P. Bull, “Extending cosmological tests of General Relativity with the Square Kilometre Array,” Astrophys. J. **817**, no. 1, 26 (2016)
- [12] Y. S. Song and O. Dore, “A step towards testing general relativity using weak gravitational lensing and redshift surveys,” JCAP **0903**, 025 (2009)
- [13] D. J. Rusin *et al.*, “The Evolution of a mass - selected sample of early - type field galaxies,” Astrophys. J. **587**, 143 (2003)
- [14] R. Reyes, R. Mandelbaum, U. Seljak, T. Baldauf, J. E. Gunn, L. Lombriser and R. E. Smith, “Confirmation of general relativity on large scales from weak lensing and galaxy velocities,” Nature **464**, 256 (2010)
- [15] Thomas E. Collett and et al, “A precise extragalactic test of General Relativity,” Science **360** (2018), 6395, 1342-1346.

- [16] R. V. Pound and G. A. Rebka, Jr., “Apparent Weight of Photons,” *Phys. Rev. Lett.* **4**, 337 (1960).
- [17] N. Ashby, “Relativity in the Global Positioning System,” *Living Rev. Rel.* **6**, 1 (2003)
- [18] E. Witten, “Bound states of strings and p-branes,” *Nucl. Phys. B* **460**, 335 (1996)
- [19] N. Seiberg and E. Witten, “String theory and noncommutative geometry,” *JHEP* **9909**, 032 (1999)
- [20] A. Connes, M. R. Douglas and A. S. Schwarz, “Noncommutative geometry and matrix theory: Compactification on tori,” *JHEP* **9802**, 003 (1998)
- [21] M. Chaichian, M. M. Sheikh-Jabbari and A. Tureanu, “Hydrogen atom spectrum and the Lamb shift in noncommutative QED,” *Phys. Rev. Lett.* **86**, 2716 (2001)
- [22] A. Kempf, G. Mangano and R. B. Mann, “Hilbert space representation of the minimal length uncertainty relation,” *Phys. Rev. D* **52**, 1108 (1995)
- [23] G. Amelino-Camelia, “Quantum-Spacetime Phenomenology,” *Living Rev. Rel.* **16**, 5 (2013)
- [24] D. Colladay and V. A. Kostelecky, “Lorentz violating extension of the standard model,” *Phys. Rev. D* **58**, 116002 (1998)
- [25] S. M. Carroll, J. A. Harvey, V. A. Kostelecky, C. D. Lane and T. Okamoto, “Noncommutative field theory and Lorentz violation,” *Phys. Rev. Lett.* **87**, 141601 (2001)
- [26] I. Antoniadis, N. Arkani-Hamed, S. Dimopoulos and G. R. Dvali, “New dimensions at a millimeter to a Fermi and superstrings at a TeV,” *Phys. Lett. B* **436**, 257 (1998)
- [27] N. Arkani-Hamed, S. Dimopoulos and G. R. Dvali, “The Hierarchy problem and new dimensions at a millimeter,” *Phys. Lett. B* **429**, 263 (1998) 5[hep-ph/9803315].
- [28] H. S. Snyder, “Quantized space-time,” *Phys. Rev.* **71**, 38 (1947).
- [29] S. Doplicher, K. Fredenhagen and J. E. Roberts, “The Quantum structure of space-time at the Planck scale and quantum fields,” *Commun. Math. Phys.* **172**, 187 (1995)
- [30] P. Nicolini, A. Smailagic and E. Spallucci, “Noncommutative geometry inspired Schwarzschild black hole,” *Phys. Lett. B* **632**, 547 (2006)
- [31] S. Ansoldi, P. Nicolini, A. Smailagic and E. Spallucci, “Noncommutative geometry inspired charged black holes,” *Phys. Lett. B* **645**, 261 (2007)
- [32] T. G. Rizzo, “Noncommutative Inspired Black Holes in Extra Dimensions,” *JHEP* **0609**, 021 (2006)
- [33] D. M. Gingrich, “Noncommutative geometry inspired black holes in higher dimensions at the LHC,” *JHEP* **1005**, 022 (2010)

- [34] S. A. Alavi, “Reissner-Nordstrom black hole in noncommutative spaces,” *Acta Phys. Polon. B* **40**, 2679 (2009)
- [35] W. Kim and D. Lee, “Bound of Noncommutativity Parameter Based on Black Hole Entropy,” *Mod. Phys. Lett. A* **25**, 3213 (2010)
- [36] A. Smailagic and E. Spallucci, “New isotropic versus anisotropic phase of noncommutative 2-D harmonic oscillator,” *Phys. Rev. D* **65**, 107701 (2002)
- [37] A. Smailagic and E. Spallucci, “UV divergence free QFT on noncommutative plane,” *J. Phys. A* **36**, L517 (2003)
- [38] A. Smailagic and E. Spallucci, “Feynman path integral on the noncommutative plane,” *J. Phys. A* **36**, L467 (2003)
- [39] E. Spallucci, A. Smailagic and P. Nicolini, “Trace Anomaly in Quantum Spacetime Manifold,” *Phys. Rev. D* **73**, 084004 (2006)
- [40] P. Nicolini and E. Spallucci, “Noncommutative geometry inspired wormholes and dirty black holes,” *Class. Quant. Grav.* **27**, 015010 (2010)
- [41] E. F. Taylor and J. A. Wheeler, “Exploring black holes,” (Addison-Wesley, 2000).
- [42] A. Farag Ali, M. M. Khalil and E. C. Vagenas, “Minimal Length in quantum gravity and gravitational measurements,” *EPL* **112**, no. 2, 20005 (2015)
- [43] T. Nakama and J. Yokoyama, “Micro black holes formed in the early Universe and their cosmological implications,” arXiv:1811.05049 [gr-qc].
- [44] I. I. Shapiro, “Fourth Test of General Relativity,” *Phys. Rev. Lett.* **13**, 789 (1964).
- [45] R. F. C. Vessot *et al.*, “Test of Relativistic Gravitation with a Space-Borne Hydrogen Maser,” *Phys. Rev. Lett.* **45**, 2081 (1980).
- [46] B. Bertotti, L. Iess and P. Tortora, ‘A test of general relativity using radio links with the Cassini spacecraft,” *Nature* **425**, 374 (2003).
- [47] C. D. Hoyle, U. Schmidt, B. R. Heckel, E. G. Adelberger, J. H. Gundlach, D. J. Kapner and H. E. Swanson, “Submillimeter tests of the gravitational inverse square law: a search for ‘large’ extra dimensions,” *Phys. Rev. Lett.* **86**, 1418 (2001)
- [48] R. D. Newman, E. C. Berg and P. E. Boynton, “Tests of the gravitational inverse square law at short ranges,” *Space Sci. Rev.* **148**, 175 (2009).